PCCP

PAPER

View Article Online
View Journal | View Issue



Cite this: *Phys. Chem. Chem. Phys.*, 2019, **21**, 17029

# Effect of light atoms on thermal transport across solid–solid interfaces

Ruiyang Li,[a] Kiarash Gordiz,[b] Asegun Henry,[b] Patrick E. Hopkins,[cde] Eungkyu Lee*[a] and Tengfei Luo*[afg]

Received 17th June 2019,
Accepted 23rd July 2019

DOI: 10.1039/c9cp03426a

rsc.li/pccp

Thermal transport across solid interfaces is of great importance for applications like power electronics. In this work, we perform non-equilibrium molecular dynamics simulations to study the effect of light atoms on the thermal transport across SiC/GaN interfaces, where light atoms refer to substitutional or interstitial defect atoms lighter than those in the pristine lattice. Various light atom doping features, such as the light atom concentration, mass of the light atom, and skin depth of the doped region, have been investigated. It is found that substituting Ga atoms in the GaN lattice with lighter atoms (*e.g.* boron atoms) with 50% concentration near the interface can increase the thermal boundary conductance (TBC) by up to 50%. If light atoms are introduced interstitially, a similar increase in TBC is observed. Spectral analysis of interfacial heat transfer reveals that the enhanced TBC can be attributed to the stronger coupling of mid- and high-frequency phonons after introducing light atoms. We have also further included quantum correction, which reduces the amount of enhancement, but it still exists. These results may provide a route to improve TBC across solid interfaces as light atoms can be introduced during material growth.



## Introduction

High-electron-mobility transistors (HEMTs) based on III–V semiconductors (*e.g.*, GaN) have attracted much research interest because of their high power and frequency capabilities.[1,2] However, the large thermal boundary resistance (TBR) across solid–solid interfaces impedes effective heat dissipation in high power electronics.[3–5] For example, the temperature in the channel of GaN-based devices can rise up to 115 °C largely due to the high GaN/substrate TBR.[6] Such overheating problem can lead to gate leakage current and carrier mobility drop. This makes efficient thermal management a crucial aspect in order to maintain the performance and reliability of microelectronic devices.

Recently several strategies have been proposed to increase the thermal boundary conductance (TBC, the reciprocal of TBR) at a solid–solid interface. High thermal conductivity substrates like SiC and diamond have been used to substitute for Si and sapphire substrates, making the interface more critical. Since the TBR is originated from the phonon spectral mismatch of two different materials, it has been proposed that one can bridge the phonon spectra by inserting a thin intermediate layer between two contacting materials.[7–11] Additionally, enlarging the interfacial contact area by introducing nanostructures to the interface was found to greatly enhance the TBC, which has been demonstrated by theoretical and experimental studies.[12–15] Moreover, the enhanced phonon scatterings near or even away from the interface were proved to be beneficial to the interfacial thermal transport if we take proper approaches such as introducing disorders and isotopes.[16,17]

It has also been theoretically proved that increasing the strength of the interfacial interatomic interaction can improve thermal transport across interfaces,[18–21] which can be attributed to the increased power exchanged between two materials. Experimentally, the effects of bond strength on TBC have been investigated in a few systems using self-assembled monolayers,[22] pressure control,[23] or surface termination[24] to tune the interfacial interactions. It is derived that the heat current from material A to material B can be expressed based on interatomic forces and velocities[25–27]

$$Q_{A\to B} = \sum_{i\in A}\sum_{j\in B} Q_{i\to j} = -\sum_{i\in A}\sum_{j\in B}\left\{\frac{\partial U_i}{\partial \boldsymbol{r}_j}\cdot \boldsymbol{v}_j - \frac{\partial U_j}{\partial \boldsymbol{r}_i}\cdot \boldsymbol{v}_i\right\}, \quad (1)$$

[a] *Department of Aerospace and Mechanical Engineering, University of Notre Dame, Notre Dame, Indiana 46556, USA. E-mail: elee18@nd.edu, tluo@nd.edu*
[b] *Department of Mechanical Engineering, Massachusetts Institute of Technology, Cambridge, Massachusetts 02139, USA*
[c] *Department of Mechanical and Aerospace Engineering, University of Virginia, Charlottesville, Virginia 22904, USA*
[d] *Department of Materials Science and Engineering, University of Virginia, Charlottesville, Virginia 22904, USA*
[e] *Department of Physics, University of Virginia, Charlottesville, Virginia 22904, USA*
[f] *Department of Chemical and Biomolecular Engineering, University of Notre Dame, Notre Dame, Indiana 46556, USA*
[g] *Center for Sustainable Energy of Notre Dame (ND Energy), University of Notre Dame, Notre Dame, Indiana 46556, USA*

where $r_i$ is the atomic position, $U_i$ is the local potential energy, and the velocities of atoms i and j are denoted by $v_i$ and $v_j$, respectively. Based on this formula, increasing atomic velocity may facilitate the interfacial energy transport as well. A recent study showed that the lighter Si interface has a greater TBC compared with that of the Ge interface.[28] It was also experimentally proved that introducing defects with smaller masses at amorphous interfaces can increase TBC.[29] However, the mechanisms underlying such enhancement and the extent of light atom effect on TBC are not fully understood.

As for the theoretical prediction of TBC, it is noted that traditional mismatch models such as diffusive mismatch model (DMM) are limited because they do not consider the inelastic phonon scatterings,[30] which means they cannot accurately include the impact of atomic interfacial features (roughness, disorder, *etc.*). On the other hand, molecular dynamics (MD) simulations, which fully include elastic and inelastic scatterings, can incorporate the influence of disorders like light atoms in the structure.[4] A previous study compared the results of nonequilibrium (NEMD) with equilibrium (EMD) molecular dynamics methods regarding the TBC at solid interfaces, and it was found that NEMD can predict the out-of-equilibrium TBC consistent with the interfacial flux describing phonon transport in each solid.[31] It has also been demonstrated that the mass mismatch of two materials can influence the interfacial thermal transport by tuning the phonon transmission.

In this study, we use MD simulations to investigate the effect of light atoms on TBC at the GaN/SiC interface, an important interface in HEMTs. We perform NEMD simulations[32] to calculate the TBC, where a portion of gallium (Ga) atoms are substituted with light atoms such as boron (B) atoms near the interface. It is found that light atoms can enhance TBC when they are introduced right at the interface. The enhancement of TBC is studied by changing the light atom concentration and the mass of the light atom while keeping the pristine potential parameters, and we show that merely introducing light atoms with the mass of boron in the first interfacial atomic layer can lead to a TBC increase by as much as 50%. Moreover, we examine the effects of other factors (*e.g.*, skin depth of the light atom-doped region) on the TBC. These results reveal that light atoms may hinder the overall thermal transport if the skin depth of the light atom-doped region is too large due to the enhanced phonon scattering in this region that lowers the local thermal conductivity. We also show that the TBC enhancement is significant even if the light atoms are introduced as interstitial additives. By calculating the spectrally decomposed TBC, we analyze the contributions of different phonon modes to the TBC. Spectral analysis indicates that high velocity light atoms introduce mid- and high-frequency phonon modes that can couple well with the counterparts on the other side of the interface, which consequently enhances the TBC.

We also acknowledge that for practical applications, GaN/SiC interfaces are generally grown with an AlN transition layer, which is necessary to grow high-quality GaN due to the lattice mismatch between GaN and SiC. However, AlN as a thermal resistive transition layer can add to the TBR, and there are issues concerning the quality of the AlN as well as the defects in the GaN near the interface which can impede heat flow.[33,34] It has been reported that techniques like surface activated bonding (SAB) can be employed to directly grow high-quality GaN on SiC, which has the potential to be widely used in the heterogeneous integration of semiconductor materials and the microelectronics packaging.[35,36] Moreover, the physics understood from this study should be generalization to any other solid–solid interfaces. Therefore, this study may provide a route to improve TBC across solid interfaces as light atoms can be introduced during material growth.

## Molecular dynamics simulation details

Fig. 1(a) depicts an example configuration for MD simulations. To understand the effect of light atoms on TBC, Ga is selected as the target element for substitution because it has the largest mass in this structure. We note light atoms may be introduced to the interface using experimental techniques like ion implantation.[37] In the doped systems, B (10.811 amu) atoms are introduced as light atoms randomly substituting for Ga (69.723 amu) in GaN with the concentration $f$:

$$f = \frac{n_l}{n_{tot}} \times 100\%, \quad (2)$$

where $n_l$ and $n_{tot}$ are the number of B atoms and the total number of atoms in each atomic layer. Besides the light atom concentration, the skin depth of the doped region $L$ (as indicated in Fig. 1a) is another important parameter, which can be used to

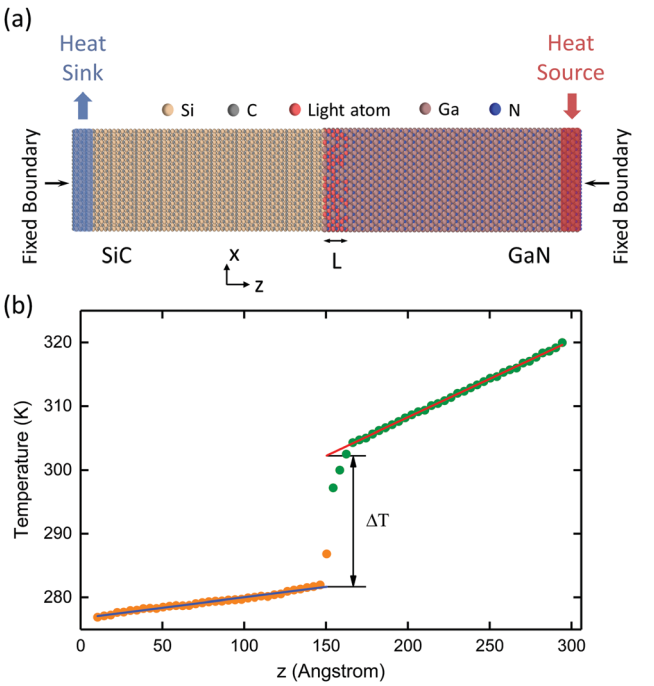


Fig. 1 (a) Structure of an example supercell and boundary conditions of a SiC/GaN interface with 50% light atoms doped in the GaN layer. (b) The calculated steady-state temperature profile as a function of the $z$-coordinate ($L$ = 15 Å).

control how many light atoms are doped during the growth of GaN. The SiC (6H–SiC) and GaN (wurtzite) layers are modeled by the Tersoff potential,[38,39] which has been previously used to study the SiC/GaN interfaces.[9,12] To isolate the mass effect, we use the same Tersoff potential parameters for GaN with and without light atoms. It is noted that simulating B atoms with potential parameters for Ga may lead to discrepancy from the reality, but in this way, we can isolate the mass effect from other factors (*e.g.*, lattice distortion, bond weakening/strengthening). At the SiC/GaN interface, the SiC layer is Si-terminated and the GaN layer is Ga-terminated. The potential for interfacial interactions is also Tersoff, and the parameters are obtained by the mixing rule.[40] In the simulations, we study the cases where GaN is epitaxially connected to SiC. The *c*-axis of the wurtzite crystal is aligned with the *z*-direction, and the numbers of unit cells for GaN and SiC are $8 \times 14 \times 30$ and $8 \times 14 \times 10$, respectively. Periodic boundary conditions are applied in all three spatial directions during relaxation, and a timestep of 0.5 fs is used for all simulations. After first relaxing the structures under isobaric–isothermal conditions (*NPT*) at 1 bar and 300 K for 3 ns, we simulate the structures in the microcanonical (*NVE*) ensemble with fixed boundary condition in the *z*-direction for 4 ns during which a steady-state temperature gradient is established and the temperatures of atoms are recorded for TBC calculation. The TBC is obtained by

$$G_{\mathrm{SiC/GaN}} = \frac{Q}{A\Delta T}, \tag{3}$$

where $Q$ is the steady-state heat current along the *z*-direction, $A$ is the cross-sectional area, and $\Delta T$ is the temperature change at the interface determined by extrapolating linear fits of the temperature profiles of the two materials to the interface and calculating the difference. A typical nonequilibrium temperature profile observed in the doped case is also shown in Fig. 1(b). It is worth mentioning that during the calculation, we always extrapolate the temperatures of the non-doped atomic layers. This guarantees that we calculate the effective TBC across the SiC/GaN interface that considers both the thermal transport right at the interface and any thermal conductivity change induced in the light atom-doped layer.

## Results and discussion

Fig. 2(a) shows the relationship between $G_{\mathrm{SiC/GaN}}$ and $L$, the skin depth of the doping region, for different concentrations, while the light atom mass is approximately equal to that of boron. As a reference, the $G_{\mathrm{SiC/GaN}}$ for the pristine SiC/GaN is also calculated ($\sim$495 MW m$^{-2}$ K$^{-1}$), which is close to reported values from other MD simulations (470–530 MW m$^{-2}$ K$^{-1}$).[12,13] The $G_{\mathrm{SiC/GaN}}$ values reported from experiments (200–250 MW m$^{-2}$ K$^{-1}$)[41] are understandably lower than our MD values due to the lattice mismatch and other defects (*e.g.*, voids and dislocations in the GaN near the interface) in real samples as well as quantum effects. Compared with the pristine case, it is obvious that $G_{\mathrm{SiC/GaN}}$ can be improved when B atoms are introduced in the vicinity of the interface, especially for the cases of higher concentration. For $f$ = 50%, one layer of B atoms can lead to a $G_{\mathrm{SiC/GaN}}$ increase by as much as 50%. However, if we dope more B atoms in the layers away from the interface, $G_{\mathrm{SiC/GaN}}$ will decrease monotonically as $L$ increases, and $G_{\mathrm{SiN/GaN}}$ can be even smaller than that of the pristine case. For $f$ = 30% and 10%, the same trend is also observed. Generally, the increase is significant when B atoms are limited within the $\sim$1 nm region from the interface. These results suggest that light atoms can increase the TBC only when the skin depth of doped region is thin. Beyond a certain distance away from the interface, the light atoms have very weak interaction with atoms on the other side of the interface, thus their higher atomic velocities do not contribute much to increasing TBC. As seen from Fig. 1(b), the doped region shows a much sharper temperature slope, which means the local thermal conductivity is significantly reduced. Therefore, the thick doped region adds additional thermal resistance to the thermal transport across the interface, reducing the effective TBC.

To confirm that the change in atomic mass is responsible for the TBC enhancement, we study $G_{\mathrm{SiC/GaN}}$ while the mass of

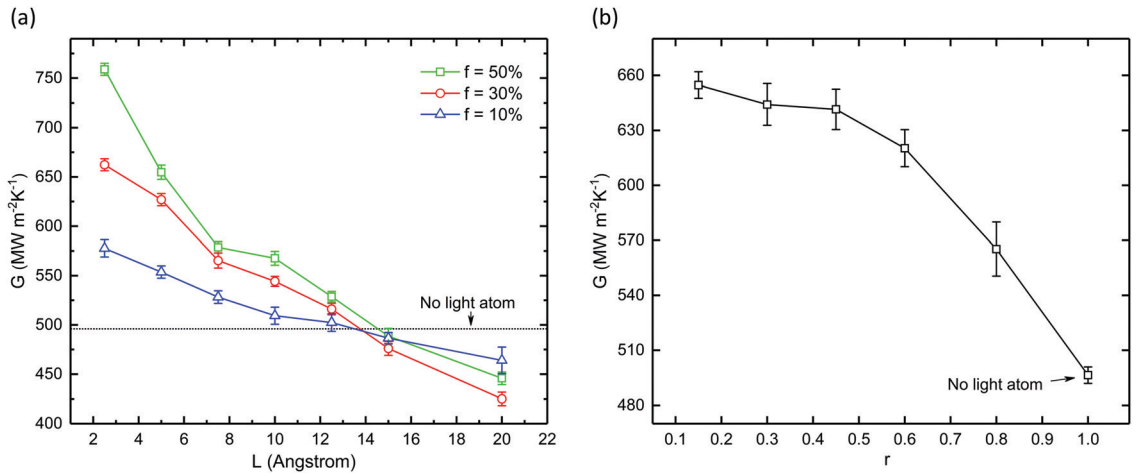


Fig. 2 (a) $G_{\mathrm{SiC/GaN}}$ ($r$ = 0.15, light atom has the mass of boron) as a function of the skin depth ($L$) of the doped region with different concentrations, where Ga are randomly substituted with light atoms. (b) $G_{\mathrm{SiC/GaN}}$ by varying $r$, the ratio of the light atom mass over the mass of Ga, with $L$ = 5 Å.

light atom is varied. The atomic mass of the light atom is set to $(r{\cdot}m_{Ga})$, where $m_{Ga}$ is the mass of Ga, and $r$ is a scaling factor. Although the scaled mass does not necessarily correspond to any realistic elements, this parametric study helps us single out the mass effect. Fig. 2(b) shows the calculated $G_{SiC/GaN}$ when $r$ changes from 0.15 to 0.8 with the fixed length of doped region $L$ of 5 Å and concentration $f$ = 50%. When $r$ = 0.15, the light atom mass approximately equals that of boron, and that is the case we discussed above. $r$ = 1.0 here refers to the pristine case. When $r$ is increased, $G_{SiC/GaN}$ keeps decreasing, and the drop is more obvious when $r$ is greater than 0.5, but all cases show $G_{SiC/GaN}$ higher than that of the pristine SiC/GaN interface. This observation suggests that the enhancement of $G_{SiC/GaN}$ is related to the mass change of atoms at the interface, and that increasing the light atom mass to approach that of Ga will diminish the benefit of light atoms.

To investigate if directly inserting light atoms interstitially near the interface also benefits the TBC, we calculate $G_{SiC/GaN}$ when B atoms are placed between GaN layers. Here, the concentration of B atom is fixed to $f$ = 10%, because adding too many interstitial atoms is found to significantly disrupt the interface structure. Similar to the trend observed in Fig. 2(a), it is found that interstitial B atoms can also lead to larger $G_{SiC/GaN}$, and $G_{SiC/GaN}$ continues to drop as the B atom-doped region is thicker (Fig. 3). This result confirms the effect of light atoms near the interface. As interstitial additives, which is also possible in experiments, light atoms can facilitate the thermal transport across GaN/SiC interfaces.

The TBC improvement can be explained by the high velocity light atoms at the interface that lead to a more efficient interfacial energy transport. At the atomic level, thermal energy is transferred across an interface by the atoms in one side doing work on the atoms in the other side.[25] As expressed in eqn (1), interfacial heat current, $Q$, can be calculated using forces and atomic velocities at the interface. At a given temperature, lighter atoms will have higher velocities than heavier atoms since their kinetic energies are the same $\left(\frac{3}{2}k_BT = \frac{1}{2}m_iv_i^2\right)$, and thus lighter atoms would increase the heat flux across the interface. The light atom-doped region, when sufficiently thin and placed properly, will lead to limited reduction in local thermal conductivity while enhance the TBC. In order to better understand the effect of light atoms on $G_{SiN/GaN}$, an analysis of the phonon modal contribution to TBC will be helpful.[26,42]

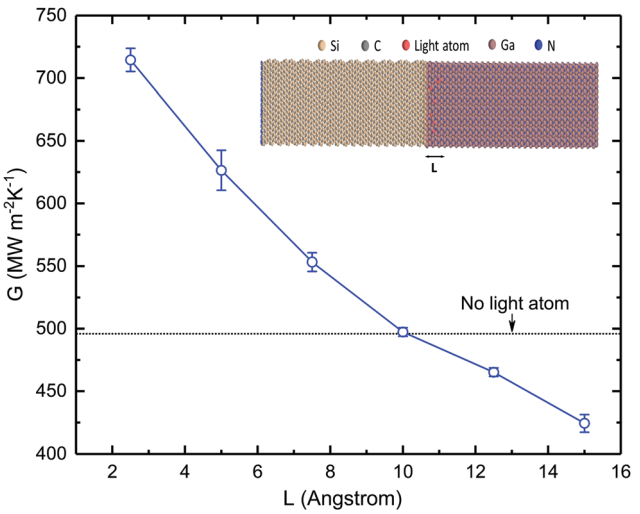


Fig. 3 $G_{SiC/GaN}$ as a function of $L$ with $f$ = 10% when boron atoms ($r$ = 0.15) are incorporated into the GaN layer as interstitial additives. The inset is a schematic of the structure.

The heat flux $Q_{A\to B}$ in eqn (1) can be decomposed spectrally as $Q_{A\to B} = \int_0^\infty \frac{d\omega}{2\pi} q_{A\to B}(\omega)$, where $\omega$ is the phonon angular frequency. The spectral heat flux $q_{A\to B}(\omega)$ is given by

$$q_{A\to B}(\omega) = 2\mathrm{Re}[\tilde{K}_{A\to B}(\omega)], \tag{4}$$

where $\tilde{K}_{A\to B}(\omega) = \int_{-\infty}^{\infty} dt e^{i\omega t} K_{A\to B}(t)$ is the Fourier transform of the force–velocity cross-correlation function defined in time-domain as[27,43]

$$K_{A\to B}(t) = -\sum_{i\in A}\sum_{j\in B}\left\langle \frac{\partial U_i}{\partial \boldsymbol{r}_j}(0)\cdot \boldsymbol{v}_j(t) - \frac{\partial U_j}{\partial \boldsymbol{r}_i}(0)\cdot \boldsymbol{v}_i(t)\right\rangle. \tag{5}$$

After obtaining the spectral heat flux $q_{A\to B}(\omega)$, we can calculate the spectral thermal conductance $g_{A\to B}(\omega)$ by

$$g_{A\to B}(\omega) = \frac{q_{A\to B}(\omega)}{A\Delta T}. \tag{6}$$

To accompany the spectral conductance, we also calculate the phonon density of states (PDOS) by taking the Fourier transform of the normalized velocity autocorrelation function,[44]

$$\rho(\omega) = \int_{-\infty}^{\infty}\sum_{j=1}^{N}\frac{\langle \boldsymbol{v}_j(0)\cdot \boldsymbol{v}_j(t)\rangle}{\langle \boldsymbol{v}_j(0)\cdot \boldsymbol{v}_j(0)\rangle}e^{i\omega t}dt. \tag{7}$$

For a fair comparison of the peak heights in PDOS, $\rho(\omega)$ is multiplied by the number of atoms in each species. Thus, spectra in Fig. 4 are proportional to the total spectral energy of each species. A system with 30% lighter B atoms ($r$ = 0.15) randomly distributed in a 5 Å-thick layer right next to the interface is studied as a representative case. The computational domain is an interfacial region within ±5 Å of the interface.

Fig. 4(a) and (b) show the calculated PDOS of SiC and GaN for the pristine case, and the PDOS of SiC, GaN and light atom for the doped case, respectively. To make the discussion clear, we divide the frequency range into three regimes: low-frequency (0–14 THz), mid-frequency (14–28 THz), and high-frequency (28–40 THz) regime. It is found that the light atoms feature some profile in the mid- and high-frequency regimes due to the smaller mass (Fig. 4(b)), which overlap with SiC in these frequency regimes. The introduction of light atom causes a damping of the PDOS peak of GaN at ~23 THz. The reduction of PDOS peak of GaN may be interpreted as an increased transmission of these phonon modes,[45] which can reduce their local population on the high temperature side. Extra peaks of GaN arise at >30 THz corresponding to the peaks of light atom, which is likely due to that the high-frequency modes originated from the light atoms are delocalized.

 

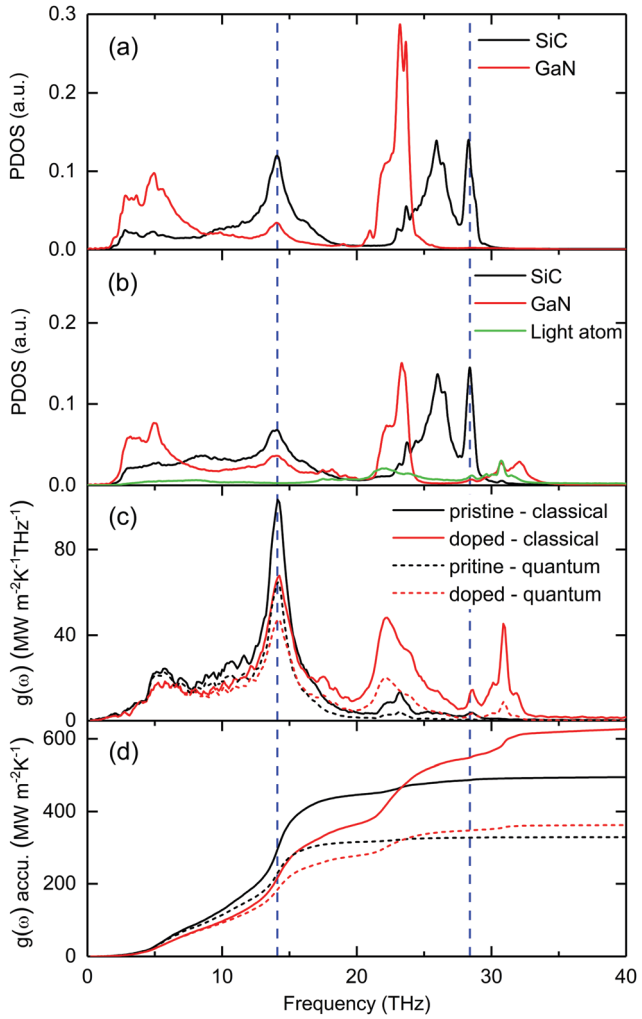


Fig. 4 The calculated phonon density of states (PDOS) for interfacial atoms in the pristine case (a) and the B-doped case (b). (c) The calculated spectral thermal conductance $g(\omega)$ before and after quantum correction for the two structures. (d) Accumulation of the spectral thermal conductance $g(\omega)$ with and without quantum correction. The whole spectrum is divided into low-frequency (0–14 THz), mid-frequency (14–28 THz), and high-frequency (28–40 THz) regimes. For the doped system here, the doping regime starts from the interface with a skin depth $L$ = 5 Å and $f$ = 30%.

Spectral thermal conductance results are shown in Fig. 4(c). Significant $g(\omega)$ peaks are observed at $\sim$14 THz for both doped and pristine cases, which is reasonable as the PDOS of the two sides overlap well around this frequency. The $g(\omega)$ of the doped system in the low-frequency range is slightly lower because some Ga are replaced with light atoms and the overall low frequency energy is reduced and shifted to higher frequency modes (*i.e.*, total energy stays the same but density of state of the doped GaN shifted to higher frequency regime). However, compared to the pristine case, there are obvious $g(\omega)$ enhancements in the mid- and high-frequency regimes for the doped system, which leads to an increase in the overall TBC. This corresponds well with the light atom PDOS spectrum in the mid- and high-frequency regimes (Fig. 4(b)), which provides better spectral overlap with SiC in these frequency regimes.

Fig. 4(d) shows the cumulative $g(\omega)$. It is found that the contribution from low-frequency phonons is smaller in the doped case compared to that in the pristine case. The TBC enhancement in the doped case mainly comes from the increased contribution of phonons in the frequency range of 16–30 THz, where the differential $g(\omega)$ of the doped case is uniformly larger than the pristine counterpart. In general, for the pristine structure, the major contribution to TBC is from low-frequency modes, which can easily carry energy across the interface due to good spectra overlap. When light atoms are introduced, low-frequency modes are moderately affected (Fig. 4(a) and (b)), but light atom will considerably enhance the coupling of mid- and high-frequency modes, resulting in a significant contribution of these phonons.

Finally, since MD simulation is in the classical limit where Boltzmann distributions are followed by phonons, we should apply certain quantum correction,[46] especially when the simulation temperature is lower than the Debye temperatures. To evaluate the efficacy of the light atom for practical HEMTs, one can correct the results by multiplying $g(\omega)$ by the factor $u^2e^u/(e^u-1)^2$, where $u = \hbar\omega/k_BT$.[47] This correction considers the overestimate of the heat capacity of high-frequency phonons, and the factor is the ratio of the quantum heat capacity (Bose distribution) to the classical one. Applying this mode-to-mode quantum correction ($T$ = 300 K) to the classical spectral conductance gives the results represented by the dashed lines in Fig. 4(c) and (d). While the overall comparison between the pristine and the doped cases for different frequency ranges still holds the same as that in the classical cases, the contribution from phonons in the frequency $>$15 THz is much smaller than the classical case. This is because the phonons in this frequency range are not significantly excited according to the Bose–Einstein distribution. The integrated conductance is understandably reduced to 328 MW m$^{-2}$ K$^{-1}$ for the pristine case and to 362 MW m$^{-2}$ K$^{-1}$ for the doped case, but the doped structure still shows $\sim$10% higher TBC compared to that of the pristine one.

## Conclusions

In conclusion, using MD simulations of SiC/GaN interfaces, we show that the introduction of light atoms (*e.g.* boron atoms) can increase TBC by as much as 50%. Investigated doping schemes may provide useful guidance to increase TBC at solid–solid interfaces in practice: (1) The enhancement is obvious only when the skin depth of the doped region is thin ($<$ 1.2 nm); (2) TBC will increase as the mass of light atom gets smaller; (3) High light atom concentration increases the TBC enhancement; (4) The enhancement is also significant for the system doped with interstitial light atoms. By analyzing the spectral thermal conductance and local PDOS, we find that light atoms increase the spectra overlap and bridge mid- and high-frequency modes in two sides. The stronger coupling of these phonon modes leads to their more significant contributions to the thermal transport across the interface. We note that in experiments, light atom like Li can be

controllably introduced as additives to the substrate during the material growth,[37] and thus the approach studied in this work may be practically applied. We also note that using more accurate potentials that can consider light atom-induced bonding change and morphology change effects is expected to lead to more accurate TBC prediction, which will be our future focus.

## Conflicts of interest

There are no conflicts to declare.

## Acknowledgements

The authors would like to thank ONR MURI (N00014-18-1-2429) for the financial support. The simulations are supported by the Notre Dame Center for Research Computing, and NSF through the eXtreme Science and Engineering Discovery Environment (XSEDE) computing resources provided by Texas Advanced Computing Center (TACC) Stampede II under grant number TG-CTS100078.

## References

1 M. Kuball, J. M. Hayes, M. J. Uren, T. Martin, J. C. H. Birbeck, R. S. Balmer and B. T. Hughes, *IEEE Electron Device Lett.*, 2002, **23**, 7–9.
2 A. L. Moore and L. Shi, *Mater. Today*, 2014, **17**, 163–174.
3 D. G. Cahill, P. V. Braun, G. Chen, D. R. Clarke, S. Fan, K. E. Goodson, P. Keblinski, W. P. King, G. D. Mahan, A. Majumdar, H. J. Maris, S. R. Phillpot, E. Pop and L. Shi, *Appl. Phys. Rev.*, 2014, **1**, 011305.
4 T. Luo and G. Chen, *Phys. Chem. Chem. Phys.*, 2013, **15**, 3389–3412.
5 E. T. Swartz and R. O. Pohl, *Rev. Mod. Phys.*, 1989, **61**, 605–668.
6 K. A. Filippov and A. A. Balandin, *MRS Internet J. Nitride Semicond. Res.*, 2014, **8**, 4.
7 T. S. English, J. C. Duda, J. L. Smoyer, D. A. Jordan, P. M. Norris and L. V. Zhigilei, *Phys. Rev. B: Condens. Matter Mater. Phys.*, 2012, **85**, 035438.
8 N. Q. Le, J. C. Duda, T. S. English, P. E. Hopkins, T. E. Beechem and P. M. Norris, *J. Appl. Phys.*, 2012, **111**, 084310.
9 E. Lee and T. Luo, *Phys. Chem. Chem. Phys.*, 2017, **19**, 18407–18415.
10 C. A. Polanco, R. Rastgarkafshgarkolaei, J. Zhang, N. Q. Le, P. M. Norris and A. W. Ghosh, *Phys. Rev. B*, 2017, **95**, 195303.
11 T. Zhang, A. R. Gans-Forrest, E. Lee, X. Zhang, C. Qu, Y. Pang, F. Sun and T. Luo, *ACS Appl. Mater. Interfaces*, 2016, **8**, 33326–33334.
12 M. Hu, X. Zhang, D. Poulikakos and C. P. Grigoropoulos, *Int. J. Heat Mass Transfer*, 2011, **54**, 5183–5191.
13 E. Lee, T. Zhang, M. Hu and T. Luo, *Phys. Chem. Chem. Phys.*, 2016, **18**, 16794–16801.
14 E. Lee, T. Zhang, T. Yoo, Z. Guo and T. Luo, *ACS Appl. Mater. Interfaces*, 2016, **8**, 35505–35512.
15 Z. Tian, K. Esfarjani and G. Chen, *Phys. Rev. B: Condens. Matter Mater. Phys.*, 2012, **86**, 235304.
16 E. Lee and T. Luo, *Appl. Phys. Lett.*, 2018, **112**, 011603.
17 L. Yates, J. Anderson, X. Gu, C. Lee, T. Bai, M. Mecklenburg, T. Aoki, M. S. Goorsky, M. Kuball, E. L. Piner and S. Graham, *ACS Appl. Mater. Interfaces*, 2018, **10**, 24302–24309.
18 T. Luo and J. R. Lloyd, *Adv. Funct. Mater.*, 2012, **22**, 2495–2502.
19 L. Hu, L. Zhang, M. Hu, J.-S. Wang, B. Li and P. Keblinski, *Phys. Rev. B: Condens. Matter Mater. Phys.*, 2010, **81**, 235427.
20 Z.-Y. Ong and E. Pop, *Phys. Rev. B: Condens. Matter Mater. Phys.*, 2010, **81**, 155408.
21 M. Shen, W. J. Evans, D. Cahill and P. Keblinski, *Phys. Rev. B: Condens. Matter Mater. Phys.*, 2011, **84**, 195432.
22 M. D. Losego, M. E. Grady, N. R. Sottos, D. G. Cahill and P. V. Braun, *Nat. Mater.*, 2012, **11**, 502–506.
23 W.-P. Hsieh, A. S. Lyons, E. Pop, P. Keblinski and D. G. Cahill, *Phys. Rev. B: Condens. Matter Mater. Phys.*, 2011, **84**, 184107.
24 K. C. Collins, S. Chen and G. Chen, *Appl. Phys. Lett.*, 2010, **97**, 083102.
25 G. Domingues, S. Volz, K. Joulain and J. J. Greffet, *Phys. Rev. Lett.*, 2005, **94**, 085901.
26 K. Sääskilahti, J. Oksanen, S. Volz and J. Tulkki, *Phys. Rev. B: Condens. Matter Mater. Phys.*, 2015, **91**, 115426.
27 Z. Fan, L. F. C. Pereira, P. Hirvonen, M. M. Ervasti, K. R. Elder, D. Donadio, T. Ala-Nissila and A. Harju, *Phys. Rev. B: Condens. Matter Mater. Phys.*, 2017, **95**, 144309.
28 K. Gordiz and A. Henry, *J. Appl. Phys.*, 2017, **121**, 025102.
29 A. Giri, S. W. King, W. A. Lanford, A. B. Mei, D. Merrill, L. Li, R. Oviedo, J. Richards, D. H. Olson, J. L. Braun, J. T. Gaskins, F. Deangelis, A. Henry and P. E. Hopkins, *Adv. Mater.*, 2018, **30**, e1804097.
30 J. T. Gaskins, G. Kotsonis, A. Giri, S. Ju, A. Rohskopf, Y. Wang, T. Bai, E. Sachet, C. T. Shelton, Z. Liu, Z. Cheng, B. M. Foley, S. Graham, T. Luo, A. Henry, M. S. Goorsky, J. Shiomi, J. P. Maria and P. E. Hopkins, *Nano Lett.*, 2018, **18**, 7469–7477.
31 S. Merabia and K. Termentzidis, *Phys. Rev. B: Condens. Matter Mater. Phys.*, 2012, **86**, 094303.
32 N. Yang, T. Luo, K. Esfarjani, A. Henry, Z. Tian, J. Shiomi, Y. Chalopin, B. Li and G. Chen, *J. Comput. Theor. Nanosci.*, 2015, **12**, 168–174.
33 J. Cho, Y. Li, D. H. Altman, W. E. Hoke, M. Asheghi and K. E. Goodson, *IEEE Compd. Semicond. Integr. Circuit Symp.*, 2012, **2012**, 1–4.
34 J. Cho, Y. Li, W. E. Hoke, D. H. Altman, M. Asheghi and K. E. Goodson, *Phys. Rev. B: Condens. Matter Mater. Phys.*, 2014, **89**, 115301.
35 O. Moutanabbir and U. Gösele, *Annu. Rev. Mater. Res.*, 2010, **40**, 469–500.
36 F. Mu, Z. Cheng, J. Shi, S. Shin, B. Xu, J. Shiomi, S. Graham and T. Suga, arXiv preprint arXiv:1905.04171, 2019.
37 M. Dalmer, M. Restle, M. Sebastian, U. Vetter, H. Hofsäss, M. D. Bremser, C. Ronning, R. F. Davis, U. Wahl and K. Bharuth-Ram, *J. Appl. Phys.*, 1998, **84**, 3085–3089.
38 P. Erhart and K. Albe, *Phys. Rev. B: Condens. Matter Mater. Phys.*, 2005, **71**, 035211.

 

39 J. Nord, K. Albe, P. Erhart and K. Nordlund, *J. Phys.: Condens. Matter*, 2003, **15**, 5649–5662.
40 J. Tersoff, *Phys. Rev. B: Condens. Matter Mater. Phys.*, 1989, **39**, 5566–5568.
41 E. Ziade, J. Yang, G. Brummer, D. Nothern, T. Moustakas and A. J. Schmidt, *Appl. Phys. Lett.*, 2015, **107**, 091605.
42 B. Ramos-Alvarado and S. Kumar, *J. Phys. Chem. C*, 2017, **121**, 11380–11389.
43 Y. Chalopin and S. Volz, *Appl. Phys. Lett.*, 2013, **103**, 051602.
44 J. M. Dickey and A. Paskin, *Phys. Rev.*, 1969, **188**, 1407–1418.
45 A. Giri and P. E. Hopkins, *Appl. Phys. Lett.*, 2014, **105**, 033106.
46 J. E. Turney, A. J. H. McGaughey and C. H. Amon, *Phys. Rev. B: Condens. Matter Mater. Phys.*, 2009, **79**, 224305.
47 Q. Waheed and O. Edholm, *J. Chem. Theory Comput.*, 2011, **7**, 2903–2909.